

## The role of surface oxidation on primary water stress corrosion cracking of Ni-base alloys

Yun Soo Lim\*, Seong Sik Hwang, Sung Woo Kim, Dong Jin Kim, Hong Pyo Kim  
Nuclear Materials Safety Research Division/Korea Atomic Energy Research Institute  
1045 Daedeok-daero, Yuseong-gu, Daejeon 305-353, Korea  
\*Corresponding author: yslim@kaeri.re.kr

### 1. Introduction

Ni-based Alloy 600 (Ni - 16 wt.% Cr - 8 wt.% Fe), which has been used extensively for structural components in nuclear power plants, is well known to be highly susceptible to primary water stress corrosion cracking (PWSCC) in the primary side environments of a primary water reactor (PWR) [1]. Another Ni-based Alloy 690 (Ni - 30 wt.% Cr - 10 wt.% Fe) has become a substitute for Alloy 600 owing to its excellent mechanical and corrosion properties. The predominant failure mode of Alloy 600 by PWSCC is known to be mostly intergranular SCC (IGSCC). Although the exact failure mechanism involved is still not well understood, there is currently rising evidence to support intergranular oxidation [2], in which oxygen diffusion into the grain boundaries can increase the degree of susceptibility to PWSCC. As a result, intergranular oxidation is responsible for grain boundary embrittlement, and therefore has a major contribution to IGSCC.

There is a noticeable difference in the intergranular oxidation behavior between Alloy 600 and Alloy 690. Alloy 690 is known to be more resistant to PWSCC than Alloy 600 due to its higher Cr content, which promotes the formation of protective films on the surface when exposed to primary water. Many studies on the surface oxidation of Alloy 600 have been performed. However, there is only limited literature on the surface oxidation of Alloy 690. The aim of the present study is to investigate the resistances of Alloy 600 and Alloy 690 to PWSCC, and to reveal the reasons for their different resistance to PWSCC in terms of surface and intergranular oxidation behavior.

### 2. Methods and Results

#### 2.1 Experimental

A mill-annealed Alloy 600 round bar with an outside diameter of 120 mm was used, and it was finally heat treated at 950 °C for 3 h. An Alloy 690 pipe with an outer diameter of 123.5 mm and a thickness of 32.5 mm was also used. It was solution annealed at 1070 °C, quenched by water, and then thermally heat treated at 715 °C for 6 h.

Compact tension (CT) and plate specimens were used in the corrosion test. CT specimens with a half inch thickness for a crack growth rate (CGR) test were

loaded in an autoclave. Before the PWSCC test, the CT specimens were pre-cracked by fatigue at a length of 2 mm in air at room temperature. The plate specimens for a surface oxidation test were polished down using 0.3  $\mu\text{m}$  alumina powders. All tests were conducted under the simulated PWR primary water conditions, that is, 1200 ppm B and 2 ppm Li in pure water at 325 °C, dissolved oxygen content below 5 ppb, and a hydrogen content of 30  $\text{cm}^3/\text{kg}$   $\text{H}_2\text{O}$ . The variation in crack length of the CT specimen during the test was estimated using a direct current potential drop method, and the stress intensity factor at a crack tip was maintained at 30  $\text{MPa}\sqrt{\text{m}}$ . The surface oxidation test using plate specimens was conducted in the same autoclave for 3600 h.

After the corrosion test, oxidized specimens were precisely characterized using scanning electron microscopy (SEM), high-resolution transmission electron microscopy (TEM), scanning TEM (STEM), and energy dispersive X-ray spectroscopy (EDS) attached to a STEM. TEM foils containing surface oxidation layers and grain boundaries were prepared with focused ion beam (FIB) milling using a dual-beam Hitachi FIB-2100 system with a  $\text{Ga}^+$  incident beam energy of 30 kV and a current of 1–5 nA. To eliminate the deformed surface layers generated from the sputtering of high-energy Ga ions, subsequent ion milling was applied with Ar ions with an incident beam energy level of 300 V at an incidence angle of 10 ° for 10 min.

A STEM/EDS analysis was carried out with a JEOL JEM-2100F (operating voltage 200 kV) equipped with an Oxford Instruments X-max 80T Silicon Drift Detector and an AZTEC analysis system (Ver. 3.1b). The STEM probe size was approximately 1 nm. The peaks of the Cr  $L_\alpha$  line (0.50 KeV) and the oxygen K line (0.52 KeV) are closely located in the EDS spectrum; there is intrinsically some overlap between these two peaks. Therefore, deconvolution of the overlapping spectral peaks was carried out for a clear determination of the oxygen and Cr constituent peaks.

#### 2.2 Results and Discussion

The microstructural aspects of Alloy 600 used in this study are shown in Figure 1. The average grain size was measured to be approximately 200  $\mu\text{m}$ . The precipitate morphology and distribution in the specimen under study are shown in Fig. 1. Owing to the final heat treatment at 950 °C for 3 h, precipitates significantly formed in the grain boundaries, as well as in the grain

interiors. The precipitates inside the grains had a needle-type shape, and those with a coarse round shape were closely distributed along the grain boundaries. From the diffraction pattern analysis on the precipitates, it was confirmed that all the precipitates were  $\text{Cr}_7\text{C}_3$ , irrespective of the locations of the precipitation.

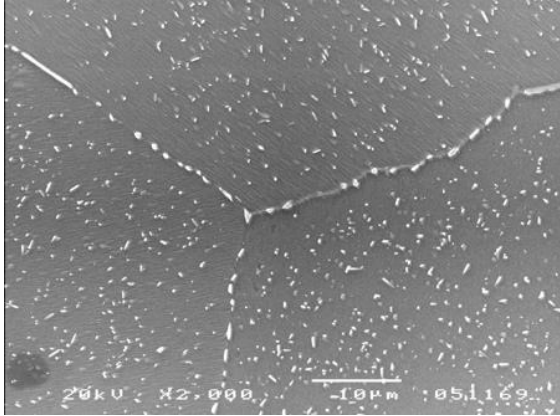


Fig. 1. SEM images on the microstructure of Alloy 600.

The microstructural features of Alloy 690 under testing were quite different from those of Alloy 600, as shown in Fig. 2. The average grain size was about  $40\ \mu\text{m}$ . In Fig. 2, only intergranular precipitates are found in this alloy without any intragranular ones. From the diffraction pattern analysis on the precipitates, it was confirmed that the intergranular precipitates were Cr-rich  $\text{M}_{23}\text{C}_6$ . Carbides precipitated during heat treatment of Alloy 690 are commonly identified as Cr-rich  $\text{M}_{23}\text{C}_6$  owing to its high Cr content.

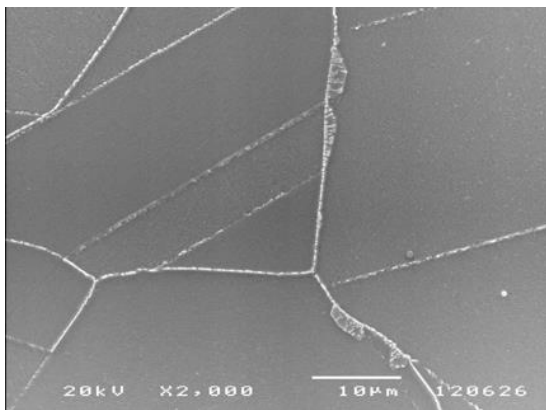


Fig. 2. SEM images on the microstructure of Alloy 690

Discontinuous precipitates are frequently found along grain boundaries in Alloy 690, as shown in Fig. 2. From the diffraction pattern analysis, it was identified that the discontinuous precipitates are also  $\text{M}_{23}\text{C}_6$  carbides and have a crystallographically parallel orientation relationship with one grain. It is known that discontinuous precipitation is associated with a concurrent grain boundary migration, and is largely dependent on the grain boundary structure [3].

The average CGR of Alloy 600 was measured to be  $7.6 \times 10^{-9}\ \text{mm/s}$  under the present conditions. This value is located in the lower bound within the range of experimental CGR data obtained under the same environment and stress conditions as ours, which means that the resistance to PWSCC is relatively high. The main reason for the high PWSCC resistance of this alloy may be caused by the intergranular Cr carbides, as shown in Fig. 1. The affirmative role of intergranular Cr carbides on the resistance to cracking has been well known [4]. Fig. 3 shows a fractured surface morphology taken from the CT specimen after the PWSCC test. In the PWSCC region, the grain shapes are clearly shown, which means that the crack propagated along the grain boundaries, thereby resulting in IGSCC. Alloy 690, however, did not crack under the normal testing conditions with crack tip blunting.

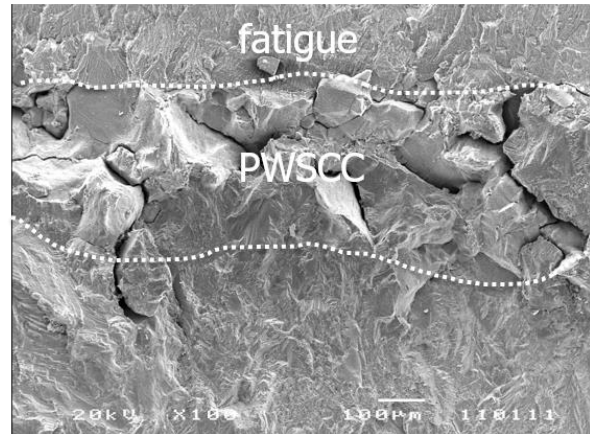


Fig. 3. Fractured surface of Alloy 600 after PWSCC test..

Metal in high-temperature water undergoes two types of damage caused by oxygen diffusing into it. Penetrated oxygen oxidizes Cr selectively on the entire surface by forming a Cr oxide, which is most likely  $\text{Cr}_2\text{O}_3$ . These surface Cr oxides act as an internal oxide layer with a thickness of a few nanometers. The grain boundaries just beneath the surface are also altered by oxygen penetration and the ensuing formation of Cr oxides. The metal then becomes prone to Cr depletion and Ni enrichment around the Cr oxides.

Fig. 4 shows a STEM image (Fig. 4(a)) and the compositional variations of O, Cr, Fe and Ni (Fig. 4(b)) across the surface of a corroded Alloy 600 specimen. These figures represent the surface oxidation layer, from which a thin continuous Cr-rich oxide layer appears to emerge. Oxygen was detected up to 38 nm deep from the surface. There seem to be at least three layers, which can be differentiated by compositional variations shown in Fig. 4(b). Other researchers [5] also reported that the surface oxidation layer of Alloy 600 consisting of multiple layers, which was very similar to our results.

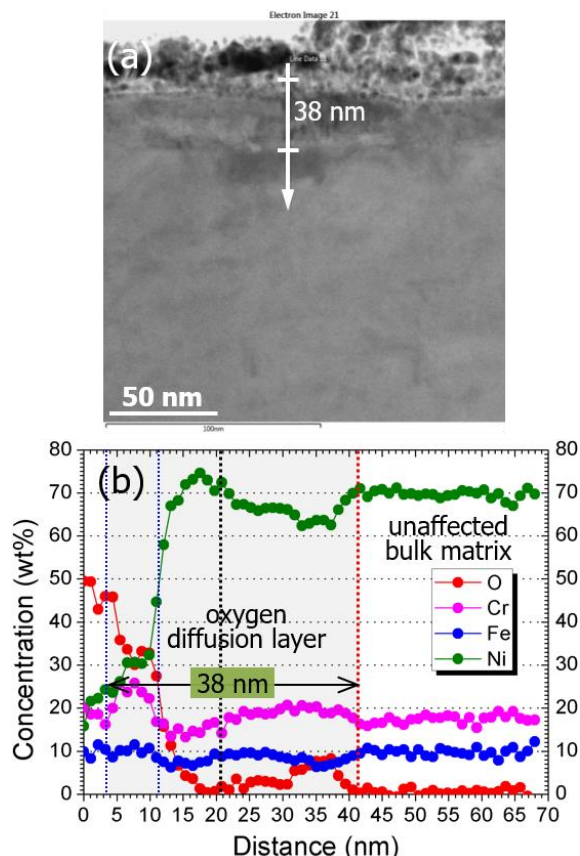


Fig. 4. (a) STEM image and (b) compositional variations of O, Cr, Fe and Ni across the surface of Alloy 600.

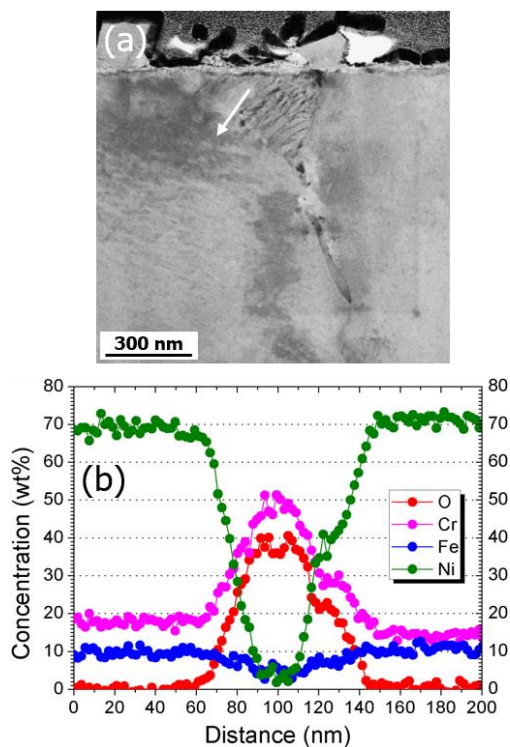


Fig. 5. (a) STEM image and (b) compositional variations of O, Cr, Fe and Ni across the surface grain boundary of Alloy 600.

In Alloy 600, oxygen diffused into the grain boundary up to about  $1 \mu\text{m}$  from the surface under the present testing condition. Fig. 5 shows a STEM image (Fig. 5(a)) and the compositional variations of O, Cr, Fe and Ni (Fig. 5(b)) across the surface grain boundary of an Alloy 600 after corrosion test. The location and direction of the measurement are denoted by an arrow in Fig. 5(a). From the line profiles across the grain boundary shown in Fig. 5(b), oxygen and Cr were strongly detected, whereas Fe and Ni were nearly completely depleted in the grain boundary. This indicates that Cr oxide formed in the oxidized grain boundary, and that Fe and Ni diffused into the outer environment. The altered structures and chemical compositions owing to the oxygen diffusion can significantly degrade the grain boundary, and increase the susceptibility to PWSCC of this alloy.

The surface oxidation layers of Alloy 690 were relatively much thicker than those of Alloy 600, as shown in Fig. 6. Fig. 6(a) shows a STEM image, and Fig. 6(b)-6(e) are compositional maps of O, Cr, Fe, and Ni. Oxygen was detected up to approximately 300 nm deep from the surface (Fig. 6(b)). The interesting feature in the figure is that there are faceted nodules outside the surface, which are composed of purely metallic Ni (Fig. 6(e)). Cr was internally oxidized and this caused the expulsion of metallic nickel nodules to the surface. Intergranular oxidation was not found in Alloy 690. This means that the intergranular oxidation was significantly suppressed in Alloy 690, unlike in the case of Alloy 600

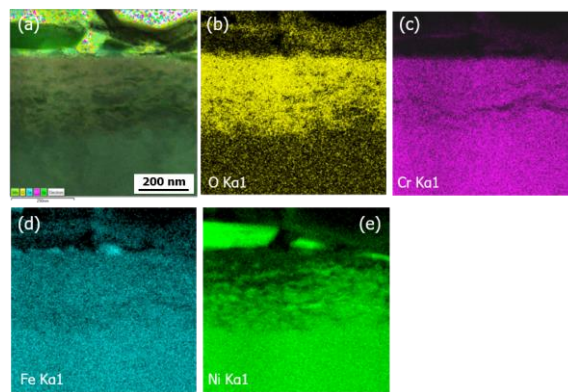


Fig. 6. (a) STEM image and composition maps of (b) O, (c) Cr, (d) Fe, and (e) Ni around the surface of Alloy 690.

Alloy 690 is known to be more resistant to IGSCC than Alloy 600 owing to its higher Cr content. The differences in the chemical compositions, especially the difference in the Cr content, may be a major factor that leads to a significant change in the intergranular oxidation behavior. The high Cr content of Alloy 690 combined with rapid diffusion along the grain boundaries allows for the development of an external  $\text{Cr}_2\text{O}_3$  type of oxide film on the surface grain boundaries.

Therefore, these considerations strongly suggest that the difference in PWSCC resistances between Alloy 600 and 690 could originate from the different behaviors of the surface and intergranular oxidation in these alloys.

### **3. Conclusions**

Alloy 600 cracked easily in normal testing conditions simulating PWR primary water, but Alloy 690 didn't. The surface grain boundaries of Alloy 600 were oxidized due to the oxygen penetration into the specimen. However, intergranular oxidation was not found in Alloy 690. The surface oxidation layers of Alloy 690 were much thicker than those of Alloy 600, and faceted nodules composed of purely metallic Ni were found outside the oxidation layer of Alloy 690. The difference in cracking susceptibilities between Alloy 600 and 690 can be attributed to the different surface and intergranular oxidation of the alloys.

### **REFERENCES**

- [1] W. Bamford and J. Hall, A review of Alloy 600 cracking in operating nuclear plants: historical experience and future trends Proc. of the 11<sup>th</sup> Int. Conf. on Environmental Degradation of Materials in Nuclear Power Systems-Water Reactor, pp. 1071-1079, 2003.
- [2] G. Bertali, F. Scenini and M.G. Burke, Advanced microstructural characterization of the intergranular oxidation of Alloy 600, Corrosion Science. Vol. 100, p. 474, 2015.
- [3] G. Gottstein and F. Schwarzer, On the orientation dependence of grain boundary energy and mobility, Materials Science Forum, Vol. 94-96, p. 187, 1992.
- [4] J. Panter, B. Viguier, J.-M. Cloué, M. Foucault and P. Combrade, E. Andrieu, Influence of oxide films on primary water stress corrosion cracking initiation of alloy 600, Journal of Nuclear Materials, Vol. 348, p. 213, 2006.
- [5] A. Clair, M. Foucault, O. Calonne and E. Finot, Optical modeling of nickel-base alloys oxidized in pressurized water reactor, Thin Solid Films, Vol. 520, p. 7125, 2012.